Available online at www.sciencedirect.com
SCIENCE DIRECT®
Journal of Sound and Vibration 275 (2004) 823–846
JOURNAL OF SOUND AND VIBRATION
www.elsevier.com/locate/jsvi

The ensemble statistics of the energy of a random system subjected to harmonic excitation

R.S. Langley*, A.W.M. Brown

Department of Engineering, University of Cambridge, Trumpington Street, Cambridge CB2 1PZ, UK

Received 18 November 2002; accepted 8 April 2003

Abstract

This paper is concerned with the ensemble statistics of the response to harmonic excitation of a single dynamic system such as a plate or an acoustic volume. Random point process theory is employed, and various statistical assumptions regarding the system natural frequencies are compared, namely: (i) Poisson natural frequency spacings, (ii) statistically independent Rayleigh natural frequency spacings, and (iii) natural frequency spacings conforming to the Gaussian orthogonal ensemble (GOE). The GOE is found to be the most realistic assumption, and simple formulae are derived for the variance of the energy of the system under either point loading or rain-on-the-roof excitation. The theoretical results are compared favourably with numerical simulations and experimental data for the case of a mass loaded plate.

1. Introduction

The response of a complex dynamic system at high frequencies can be predicted by using statistical energy analysis (SEA) [1], in which the system is considered to be an assembly of ''subsystems''. By considering power conservation, the method leads to a prediction of the mean vibrational energy of each subsystem. This mean value is strictly an average over an ensemble of systems with random parameters, although it is often justifiable to reinterpret this as a frequency average for any one particular system. There is much interest in predicting not only the mean energy of each subsystem but also the higher order statistics, such as the variance, but this is a highly complex task and as yet there is no reliable way in which it can be done. In this paper a number of the underlying issues are investigated for the relatively simple case of a single

*Corresponding author. Tel.: +44-1223-766-385; fax: +44-1223-332-662.
E-mail address: RSL21@eng.cam.ac.uk (R.S. Langley).

0022-460X/$ - see front matter © 2003 Elsevier Ltd. All rights reserved.
doi:10.1016/S0022-460X(03)00780-6

subsystem, such as a plate or an acoustic volume, with the aim of predicting the ensemble variance at a fixed frequency.

Some of the earliest work on the statistics of the response of a single subsystem occurred in the field of room acoustics. For example, Schroeder [2] considered the point-to-point transfer function of an acoustic volume, and concluded that at a sufficiently high frequency the real and imaginary parts are uncorrelated Gaussian random variables of equal variance. This implies that the modulus squared transfer function has an exponential distribution, from which it follows that the standard deviation is equal to the mean value. This problem was reconsidered by Lyon [3], under the assumption that the system natural frequencies form a Poisson point process. The standard deviation of the modulus squared transfer function was found to be greater than that predicted by Schroeder [2], but to reduce to the Schroeder result at very high frequencies. Lyon [3] also considered the statistics of the energy of a subsystem subjected to point loading, and furthermore considered the effect of non-Poisson natural frequencies by employing an alternative empirically based model. This work was extended by Davy [4] to the case where there are a specified number of excitation points and the response is averaged over a specified number of receive points. The assumptions made by Lyon [3] and Davy [4] regarding the statistics of the natural frequencies are now known to be invalid for most systems, and there has been much subsequent fundamental work, reported mainly in the physics literature, regarding the statistics of the spacings between neighbouring natural frequencies.

Work on random matrix theory has investigated in detail the statistical properties of the natural frequencies of a particular type of random matrix known as the Gaussian Orthogonal Ensemble (GOE) [5]. The GOE concerns a symmetric matrix whose entries are Gaussian, zero mean, and statistically independent, with the off-diagonal entries having a common variance, and the diagonal entries having twice this variance. It is known that the spacings between the eigenvalues have a Rayleigh distribution (referred to as the Wigner distribution in the random matrix literature). This contrasts with the exponential distribution that would be obtained were the natural frequencies to form a Poisson point process. A surprising fact has emerged from numerical and experimental studies: most physical systems have natural frequencies that conform to the GOE statistics, even though the random matrices that govern their behaviour have no obvious direct connection with the GOE. This has been shown experimentally for a metal block by Weaver [6], for a quartz block by Ellegaard et al. [7], and for plates by Bertlesen et al. [8]; furthermore, much numerical evidence is quoted by Mehta [5]. The GOE statistics no longer apply however when the system has ''symmetries''—in fact if the system has many symmetries (and the natural frequencies from all symmetry classes are superposed) then the Poisson spacing statistics are obtained, and this situation applies to a perfectly rectangular simply supported plate or a perfectly box-shaped room. In this case the Lyon [3] statistical assumptions are correct, but any slight perturbation of the system will disturb the symmetry and result in GOE statistics. Thus GOE statistics are to be expected for practical systems, and Weaver [9] extended the work of Lyon [3] and Davy [4] to this case, making certain simplifying assumptions in the process. These assumptions were lifted by Lobkis et al. [10] for the case of the point-to-point transfer function, although some discrepancy with experimental measurements was reported.

One effect of the approximations employed by Weaver [9] is that the subsystem energy is predicted to have zero variance when rain-on-the-roof excitation is employed. Since rain-on-the-roof excitation is commonly assumed in SEA this issue requires further investigation. In the

present work the statistics of the energy of a subsystem is investigated for both point loading and rain-on-the-roof excitation, and for comparison the point-to-point transfer function is also briefly considered. Three analytical models are investigated: Poisson natural frequency spacings, statistically independent Rayleigh natural frequency spacings, and full GOE natural frequency statistics. The separate consideration of independent Rayleigh spacings allows the effect of the spacing correlations predicted by the GOE to be investigated. The analytical models are compared with numerical simulations and experimental results for a mass loaded plate, and the GOE model is found to provide very good predictions.

2. Energy statistics

2.1. General considerations

For a proportionally damped dynamic system, the transfer function H at frequency ω between a drive point at $\mathbf{x}_0$ and a response point at $\mathbf{x}$ can be written in the form of a modal sum, so that

$$H(\omega, \mathbf{x}_0, \mathbf{x}) = \sum_n \frac{\phi_n(\mathbf{x})\phi_n(\mathbf{x}_0)}{(\omega_n^2 - \omega^2 + \mathrm{i}\eta\omega\omega_n)}, \tag{1}$$

where ϕ_n is the nth mode shape (scaled to unit generalized mass), ω_n is the nth natural frequency and η is the loss factor. The following analysis is concerned with the statistics of the response of a random system, so that both the mode shapes and the natural frequencies are random quantities when viewed across an *ensemble* of random structures. A brief analysis of the point-to-point transfer function is presented in Section 3, but the main concern is with the statistics of the time averaged (in the sense of being averaged over a cycle of harmonic vibration) kinetic energy density of the system, which for the case of a unit point load applied at $\mathbf{x}_0$ is given by

$$T(\omega) = \frac{\omega^2}{4R}\int_R \rho(\mathbf{x})|H(\omega, \mathbf{x}_0, \mathbf{x})|^2 \,\mathrm{d}\mathbf{x}. \tag{2}$$

Here R is the area (or equivalent) of the system and $\rho(\mathbf{x})$ is the mass density in appropriate units. By substituting Eq. (1) into Eq. (2), the resulting double summation can be reduced to a single summation by applying mode shape orthogonality, which yields

$$T(\omega) = \sum_n \frac{\omega^2 a_n}{[(\omega_n^2 - \omega^2)^2 + (\eta\omega\omega_n)^2]}, \tag{3}$$

where

$$a_n = \phi_n^2(\mathbf{x}_0)/4R. \tag{4}$$

For different types of loading, for example multiple point forces or rain-on-the-roof excitation, Eq. (3) will still apply but Eq. (4) will be modified. The following analysis is applicable to a general set of coefficients a_n, and thus Eq. (4) will *not* be assumed in general.

Clearly the statistical distribution of $T(\omega)$ as given by Eq. (3) is determined by the statistics of the natural frequencies of the system and also by the statistics of the numerators a_n, and this problem has been studied in detail by Lyon [3]. Apart from the first few modes, it is reasonable to assume that for each mode the modal bandwidth is small in comparison to the natural frequency,

in which case the following approximation can be applied:

$$(\omega_n^2 - \omega^2)^2 + (\eta\omega\omega_n)^2 \approx 4\omega^2(\omega_n - \omega)^2 + (\eta\omega^2)^2. \tag{5}$$

Eq. (3) can then be expressed in the form

$$T(\omega) = \sum_n a_n g(\omega_n - \omega), \tag{6}$$

$$g(\omega_n - \omega) = \frac{\omega^2}{[4\omega^2(\omega_n - \omega)^2 + (\eta\omega^2)^2]}. \tag{7}$$

The main reason for rewriting Eq. (3) in the form of Eq. (6) is that the latter equation (at fixed ω) is more amenable to analysis by using random point process theory [11,12] and three distinct cases are considered in what follows.

2.2. Poisson natural frequency spacings

Perhaps the simplest assumption regarding the system natural frequencies is that they form a Poisson point process [12]; this means that the spacings between successive natural frequencies are statistically independent and have an exponential distribution. In this case, the statistics of Eq. (6) can be derived by using Campbell's Theorem [12,13]. In particular, the mean and variance of T have the form

$$\mu_T = E[T] = 2E[a_n] \int_0^\infty v g(\Omega)\, \mathrm{d}\Omega, \tag{8}$$

$$\sigma_T^2 = \mathrm{Var}[T] = 2E[a_n^2] \int_0^\infty v g^2(\Omega)\, \mathrm{d}\Omega, \tag{9}$$

where v is the modal density of the system, and it has been assumed that the coefficients a_n are identically distributed and statistically independent of the natural frequencies. Here the symbol $E[\,]$ is used to represent an average taken over the ensemble of random structures at a fixed excitation frequency. Evaluating the integrals in Eqs. (8) and (9) gives

$$\mu_T = \frac{E[a_n]\pi v}{2\eta\omega}, \quad \sigma_T^2 = \frac{E[a_n^2]\pi v}{4\eta^3\omega^3}. \tag{10, 11}$$

The relative standard deviation, r_T say, is therefore

$$r_T^2 = (\sigma_T/\mu_T)^2 = \alpha/\pi m, \quad m = \omega\eta v, \tag{12, 13}$$

where m is the modal overlap factor, and α is given by

$$\alpha = E[a_n^2]/E[a_n]^2. \tag{14}$$

Eqs. (12)–(14) are a restatement of Eq. (23) of Ref. [3].

Eqs. (8) and (9) represent the first two cumulants of the energy T; more generally, an expression for the jth cumulant κ_j can be found by employing Eq. (4-88) of Lin [12], which gives

$$\kappa_j = 2E\,[a_n^j] \int_0^\infty v g^j(\Omega)\, \mathrm{d}\Omega. \tag{15}$$

Substituting Eq. (7) into this expression then yields

$$\kappa_j = E[a_n^j]\frac{(2j-2)!}{[(j-1)!]^2}\,2^{-2j+1}\pi v(\omega\eta)^{2j-1}. \tag{16}$$

When normalized by the standard deviation σ_T this result becomes

$$\kappa_j/\sigma_T^j = \frac{E[a_n^j]}{E[a_n^2]^{j/2}}\frac{(2j-2)!}{[(j-1)!]^2}\,2^{1-j}(\pi m)^{-j/2+1}. \tag{17}$$

The probability density function of the energy can be expanded in the form of an Edgeworth series, in which the first term is a Gaussian distribution and the amplitudes of the subsequent terms depend upon the normalized cumulants κ_j/σ_T^j, $j \geqslant 3$ [13]. Clearly, the normalized cumulants tend to zero with increasing modal overlap m, and this suggests that the energy might become Gaussian at large m. However, the behaviour of $E[a_n^j]$ with increasing j is also a relevant issue, and this in turn depends upon the type of loading considered. Furthermore, Eq. (17) is based on Poisson natural frequency spacings and this is of doubtful validity for many practical systems, as discussed in what follows.

The Poisson process model adopted in the present section is analytically convenient, but of limited practical relevance. This is because "repulsion" between modes leads to a low probability of very closely spaced natural frequencies, whereas the Poisson exponential model of the modal spacing implies that close spacings are highly probable. Lyon [3] investigated this issue by considering a spacing density function proportional to $z\exp(-vz)$ (the "nearest neighbour" distribution), where z is the natural frequency spacing; however it is now known that many practical systems have a Rayleigh spacing distribution, in line with the Wigner surmise associated with the GOE in random matrix theory [5]. Weaver [9] has derived an approximate expression for the relative variance of the energy density based on GOE statistics, valid for the case of large modal overlap, and the result has the form

$$r_T^2 = \frac{1}{LN} + \frac{1}{\pi m}\left\{\left(\frac{K}{N}+1-\frac{1}{N}\right)\left(\frac{K}{L}+1-\frac{1}{L}\right) - \frac{2}{LN} - 1\right\}, \tag{18}$$

where K is given by

$$K = E[\phi_n^4]/E[\phi_n^2]^2 \tag{19}$$

and L and N are, respectively, the number of independent receiver and source positions used in the calculation of the energy density (i.e., the energy density is averaged over L spatial points, and there are N statistically independent point forces). The result can be compared directly with Eq. (12) for the case of large L (i.e., the energy density is averaged over the whole system) and a single point load ($N = 1$), in which case $a_n = \phi_n^2$ and $\alpha = K$. The result is

$$r_T^2 = (\alpha - 1)/\pi m, \tag{20}$$

which clearly differs from Eq. (12). For the case where both L and N are large (i.e., the kinetic energy density is averaged over the whole system, under rain-on-the-roof forcing) Eq. (18) breaks down and predicts $r_T = 0$. The issue of non-Poisson natural frequency spacings is considered in detail in the following sections, and an alternative to Eq. (18) is derived which covers the problem case of large L and N. Firstly the case of statistically independent Rayleigh natural frequency spacings is considered (Section 2.3), and the analysis is then extended to include the spacing

correlations associated with the GOE (Section 2.4). It is known that most practical systems will follow the GOE, and the case of independent Rayleigh natural frequency spacings is highly unlikely to arise in practice; however a separate consideration of the latter case enables the role and importance of spacing correlations to be clearly identified.

2.3. Statistically independent Rayleigh natural frequency spacings

Stratonovich [11] has considered the statistics of a sum in the form of Eq. (6) for the case where the spacings between the points ω_n are statistically independent but have any specified distribution. The previous result for the mean of the sum, Eq. (8), still applies, but the variance is modified. The original analysis by Stratonovich is limited to the case $a_n = 1$, but this is extended to the general case in what follows. If the random function $\xi(\omega)$ is defined as

$$\xi(\omega) = \sum_{j=1}^{\infty} a_n \delta(\omega - \omega_j), \tag{21}$$

where $\delta(\omega)$ is the dirac delta function, then Eq. (6) can be rewritten as

$$T(\omega) = \int_{-\infty}^{\infty} g(\omega' - \omega)\, \xi(\omega')\, \mathrm{d}\omega'. \tag{22}$$

If the pulse sequence in Eq. (21) is a stationary random process, it follows that

$$S_T(\theta) = |F(\theta)|^2 S_\xi(\theta). \tag{23}$$

Here $S_T(\theta)$ is the spectral density of $T(\omega)$, and $S_\xi(\theta)$ is the spectral density of $\xi(\omega)$. The function $F(\theta)$ is the Fourier transform of $g(\Omega)$, so that

$$F(\theta) = \int_{-\infty}^{\infty} g(\omega' - \omega)\exp(-\mathrm{i}\theta\omega')\, \mathrm{d}\omega'. \tag{24}$$

Substituting Eq. (7) into Eq. (24) yields

$$F(\theta) = \frac{\pi}{2\eta\omega}\exp[-\eta\omega|\theta|/2 - \mathrm{i}\theta\omega]. \tag{25}$$

The spectral density $S_\xi(\theta)$ has been derived by Stratonovich [11] for the particular case $a_n = 1$; this analysis can readily be modified for the more general case to yield

$$S_\xi(\theta) = \left(\frac{\nu}{2\pi}\right)\left\{E[a_n^2] + 2E[a_n]^2 \mathrm{Re}\left(\frac{M(\theta)}{1 - M(\theta)}\right)\right\}, \tag{26}$$

where $M(\theta)$ is the characteristic function associated with the probability density function of the natural frequency spacings, $p(z)$, so that

$$M(\theta) = \int_0^{\infty} p(z)\exp(\mathrm{i}\theta z)\, \mathrm{d}z. \tag{27}$$

Eq. (26) does not include the delta function at the origin associated with the mean value of $\xi(\omega)$, and thus it follows from Eq. (23) that the *variance* of the energy can be written as

$$\sigma_T^2 = 2\int_0^{\infty} |F(\theta)|^2 S_\xi(\theta)\, \mathrm{d}\theta. \tag{28}$$

Given that the mean value of the energy is given by Eq. (10), the relative variance can be written in the form

$$r_T^2 = \frac{1}{\pi v}\int_0^\infty \left\{\alpha + 2\,\mathrm{Re}\left(\frac{M(\theta)}{1-M(\theta)}\right)\right\}\exp(-\eta\omega\theta)\,\mathrm{d}\theta, \tag{29}$$

where the spatial factor α is defined by Eq. (14). For Poisson natural frequency spacings $p(z)$ is an exponential function and hence $M(\theta) = (1 - \mathrm{i}\theta/v)^{-1}$; in this case only the first term in Eq. (29) makes a non-zero contribution and Eq. (12) is recovered, in agreement with the analysis of the previous section. In contrast, if the Wigner surmise is adopted then the natural frequency spacings have a Rayleigh distribution, in which case

$$p(z) = \frac{z}{\beta}\exp\left(-\frac{z^2}{2\beta}\right), \tag{30}$$

where $\beta = 2/(\pi v^2)$. In this case $M(\theta)$ can be expressed in terms of the incomplete gamma function P, so that

$$M(\theta) = 1 - \mathrm{i}|\theta|\sqrt{\frac{\pi b}{2}}\exp\left(-\frac{1}{2}\theta^2 b\right)\left\{1 - P\left(\frac{1}{2}, -\frac{\theta^2 b}{2}\right)\right\} \tag{31}$$

and Eq. (29) can then be evaluated by numerical integration, given a value of the factor α. The determination of α is discussed in the Section 2.5.

Eq. (29) yields the relative variance of the response for the case where the spacings between the natural frequencies have a Rayleigh distribution and are statistically independent. The Rayleigh distribution is consistent with the statistics yielded by the GOE in random matrix theory, but it should be noted that the GOE does not predict that the spacings are statistically independent. Eq. (18), given by Weaver [9], and Eq. (29) are therefore based on different assumptions, and the following section considers a more complete model of the GOE spacing statistics.

2.4. GOE natural frequency statistics

The analysis of the previous section considered the case of statistically independent Rayleigh natural frequency spacings, which partially captures the spacing statistics predicted by the GOE, although the correlations between the spacings are neglected. The effect of these correlations can be included by modifying the result for the spectrum of the random process $\xi(\omega)$, Eq. (26). Firstly, it can be noted that Lin (Ref. [12], Eq. (4-101) has given a general expression for the spectrum of $\xi(\omega)$ which, when adjusted to give zero mean, has the form

$$S_\xi(\theta) = (1/2\pi)\,\{E[a_n^2]g_1 + E[a_n]^2 G_2(\theta)\}, \tag{32}$$

where

$$G_2(\theta) = \int_{-\infty}^{\infty} g_2(\omega)\exp(-\mathrm{i}\theta\omega)\,\mathrm{d}\omega. \tag{33}$$

Here g_1 and g_2 are the first two cumulant functions of the random point process. The first, g_1, is the mean rate at which natural frequencies occur, i.e., the modal density v. The second, g_2, is determined by the higher order statistics of the frequency spacings. In brief, $g_2 = f_2 - v^2$, where $f_2(\omega)\,\mathrm{d}\omega_1\,\mathrm{d}\omega_2$ is the probability that a natural frequency occurs in each of two small frequency

intervals $d\omega_1$ and $d\omega_2$ that are separated by a frequency ω. The function g_2 is defined in a very similar way to the "two-level cluster" function Y_2 that is employed in random matrix theory [5]. In fact, apart from a sign change, Y_2 is the value taken by g_2 when the point process is scaled to give $g_1 = 1$, so that

$$g_2(\omega) = -v^2 Y_2(v\omega). \tag{34}$$

The Fourier transform of the two-level cluster function is given by Mehta [5] as

$$b(\theta) = \int_{-\infty}^{\infty} Y_2(r)\exp(-2\pi i r\theta)\,dr = \begin{cases} 1 - 2|\theta| + |\theta|\ln(1 + 2|\theta|), & |\theta| \leqslant 1, \\ -1 + |\theta|\ln\left(\dfrac{2|\theta| + 1}{2|\theta| - 1}\right), & |\theta| \geqslant 1 \end{cases} \tag{35}$$

and thus

$$G_2(\theta) = -vb(\theta/2\pi v). \tag{36}$$

Eqs. (10), (28), (32) and (36) then lead to an expression for the relative variance in the form

$$r_T^2 = \frac{1}{\pi v}\int_0^{\infty} \{\alpha - b(\theta/2\pi v)\}\exp(-\eta\omega\theta)\,d\theta. \tag{37}$$

The integral involved in the above equation can be evaluated to yield

$$r_T^2 = \frac{1}{\pi m}\left\{\alpha - 1 + \frac{1}{2\pi m}[1 - \exp(-2\pi m)] + E_1(\pi m)\left[\cosh(\pi m) - \frac{1}{\pi m}\sinh(\pi m)\right]\right\}, \tag{38}$$

where m is the modal overlap factor, and E_1 is the exponential integral [14]

$$E_1(x) = \int_x^{\infty} \frac{\exp(-t)}{t}\,dt. \tag{39}$$

The exponential integral can be expanded for large arguments (formula 5.1.51 of Ref. [14]) to yield a simple approximation to Eq. (38) in the form

$$r_T^2 \approx (\alpha - 1)/\pi m + 1/(\pi m)^2. \tag{40}$$

This approximation is correct up to second order in $1/(\pi m)$, i.e., the next term in the series is of order $1/(\pi m)^3$, and thus the expansion can be expected to be accurate down to fairly small values of m, say $m > 0.6$. For the case of a point load ($\alpha = K$), the first term in Eq. (40) agrees with the result due to Weaver [9], Eq. (20), and the relative variance is proportional predominantly to $1/(\pi m)$. For rain on the roof forcing ($\alpha = 1$), Eq. (40) states that the relative variance has a quite different behaviour, being proportional to $1/(\pi m)^2$. These results are compared with numerical simulations and experimental measurements in Sections 4 and 5, respectively.

It can be noted that for Poisson natural frequency spacings it was possible to derive an expression for the nth cumulant of the response, in the form of Eq. (16). For more general natural frequency statistics a difficulty arises in that the nth cumulant depends upon the jth cumulant function g_j of the underlying point process, for all $j \leqslant n$, as shown for example by Lin [12]. For a Poisson process only g_1 is non-zero, and hence the analysis becomes particularly straightforward. For independent Rayleigh natural frequency spacings, or GOE natural frequency statistics, the cumulant function g_j is generally non-zero, and is moreover of very complex form for $j > 2$ (see for example Eq. (6.4.20) of Mehta [5] for the case of the GOE). For this reason the analysis of this

section and the previous section is limited to the variance of the response, although at least in principle an extension could be made to higher order cumulants.

2.5. The spatial factor α

All of the results that have been derived for the relative variance of the response depend upon the spatial factor α, which is defined by Eq. (14). The term a_n that appears in this equation is the coefficient of the nth term in the modal expansion of the response, Eq. (6), and it depends upon both the nth mode shape of the system and the type of loading considered. For the case of a single point load a_n is given by Eq. (4), and hence $\alpha = K$ where K is given by Eq. (19). In conjunction with the assumption of Poisson natural frequency spacings, Lyon [3] considered the mode shapes to be a product of sine functions, in which case $K = 2.25$ is obtained for a two-dimensional system such as a plate. In contrast, for GOE statistics it is normally assumed that the mode shape at a fixed point is a Gaussian random variable (see, for example, Refs. [15,16]), in which case $K = 3$. With these values it can be seen that the Lyon [3] and Weaver [9] predictions for the relative variance under point loading are surprisingly similar: Eq. (12) yields $2.25/(\pi m)$ for the Poisson case, whereas Eq. (20) yields $2/(\pi m)$ for the GOE case. The present GOE result, Eq. (40), is $2/(\pi m) + 1/(\pi m)^2$, which is again very similar providing the modal overlap is greater than unity. For a three-dimensional system such as an acoustic volume, the Lyon value of K is 27/8, and the difference between the Lyon [3] and Weaver [9] predictions is more marked.

If more than one point load is applied then a_n becomes

$$a_n = (1/4R)\left|\sum_{j=1}^{N} f_j \phi_n^2(\mathbf{x}_j)\right|^2, \tag{41}$$

where N is the number of point loads and $\mathbf{x}_j$ and f_j are, respectively, the location and the complex amplitude of the jth point load. If the N complex amplitudes are taken to be random and statistically independent, with each having an average modulus squared value of unity, then a_n can be averaged over all possible realizations of the loading to give

$$a_n = (1/4R)\sum_{j=1}^{N} \phi_n^2(x_j). \tag{42}$$

By assuming that the mode shapes are statistically independent at the various loading points, it can readily be shown that

$$\alpha = E[a_n^2]/E[a_n]^2 = (K-1)/N + 1. \tag{43}$$

For the case $N = \infty$ and the above result yields $\alpha = 1$. In this case the various predictions of the relative variance yield very different results: the Poisson result, Eq. (12), yields $1/(\pi m)$, the Weaver GOE result, Eq. (18), yields zero, and the present GOE result, Eq. (40), yields $1/(\pi m)^2$.

In deriving Eq. (42) from Eq. (41), the coefficient a_n (and hence the energy T) has been averaged over all possible realizations of the loading *prior* to considering the ensemble statistics of T. An alternative is to allow just one realization of the loading for each realization of the random structure, so that no prior averaging over the loading is performed. If each point load is taken to have unit amplitude but random phase, so that $f_j = \exp(\mathrm{i}\theta_j)$ where θ_j has a uniform distribution

from 0 to 2π, then it can be shown that

$$\alpha = (K-2)/N + 2. \tag{44}$$

Clearly Eq. (44) is very different to Eq. (43), and in the limiting case $N = \infty$ the value $\alpha = 2$ rather than $\alpha = 1$ is obtained. This highlights the fact that when considering the variance of the energy it is important to clearly define the ensemble that is being employed. In what follows "rain-on-the-roof" is taken to describe the case in which a_n is averaged over the possible realizations of the loading, so that Eq. (43) applies.

It has been suggested in the literature (see for example Lobkis et al. [10]) that the GOE result $K = 3$ yields an overestimate of K for practical systems. This issue is explored in Section 4 by comparing relative variance predictions with numerical simulations, and also by computing K directly for an ensemble of random structures.

3. The point-to-point transfer function

By analogy with the analysis of Section 2.1, the complex point-to-point transfer function given by Eq. (1) can be rewritten in the approximate form

$$H(\omega, \mathbf{x}_0, \mathbf{x}) = H_R + \mathrm{i}H_I, \tag{45}$$

$$H_R = \sum_n c_n g_R(\omega_n - \omega), \quad g_R(\Omega) = 2\omega\Omega/(4\omega^2\Omega^2 + \eta^2\omega^4), \tag{46,47}$$

$$H_I = \sum_n c_n g_I(\omega_n - \omega), \quad g_I(\Omega) = \eta\omega^2/(4\omega^2\Omega^2 + \eta^2\omega^4), \tag{48,49}$$

where $c_n = \phi_n(\mathbf{x}_0)\phi_n(\mathbf{x})$. Eqs. (46) and (48) are in a form amenable to analysis by random point process theory, but the present aim is not to derive the statistics of H in detail, but rather to indicate the extent of previous work in this area. Firstly, it can be noted that the first two cumulants of either H_R or H_I are given by [12]

$$\kappa_1 = 2E[c_n]\int_0^\infty v g(\Omega)\,\mathrm{d}\Omega, \tag{50}$$

$$\kappa_2 = 2E[c_n^2]\int_0^\infty v g^2(\Omega)\,\mathrm{d}\Omega + E^2[c_n]\int_{-\infty}^\infty\int_{-\infty}^\infty g_2(\Omega_1 - \Omega_2)g(\Omega_1)g(\Omega_2)\,\mathrm{d}\Omega_1\,\mathrm{d}\Omega_2, \tag{51}$$

where $g(\Omega)$ represents $g_R(\Omega)$ or $g_I(\Omega)$ as appropriate, and g_2 is the second cumulant of the natural frequency point process. Now given the definition of c_n, it is reasonable to assume that $E[c_n] = 0$ apart from the special case where the drive and receive points coincide (i.e., $\mathbf{x}_0 = \mathbf{x}$). Under this assumption the first cumulant is zero, and the second cumulant is independent of g_2, which implies that the Poisson, independent Rayleigh spacing, and GOE models of the natural frequencies will all yield the same result. It can readily be shown that

$$\sigma^2_{H_R} = \sigma^2_{H_I} = E[c_n^2]\pi v/(4\eta\omega^3). \tag{52}$$

Furthermore, the second order joint cumulant between the real and imaginary parts of the transfer function can be shown to be proportional to the integral of the product $g_R(\Omega)g_I(\Omega)$ along

the real axis, from which it follows that $E[H_R H_I] = 0$. These results are fully consistent with results derived by Schroeder for the point-to-point transfer function of a room [2]. Schroeder further assumed that H_R and H_I are Gaussian, so that a transformation of variables leads to the results

$$p(|H|) = \frac{|H|}{\sigma_{H_R}^2} \exp\left(-\frac{|H|^2}{2\sigma_{H_R}^2}\right), \quad p(\varphi) = \left(\frac{1}{2\pi}\right), \tag{53, 54}$$

$$p(|H|^2) = \frac{1}{2\sigma_{H_R}^2} \exp\left(-\frac{|H|^2}{2\sigma_{H_R}^2}\right), \tag{55}$$

where $|H|$ is the modulus of the complex transfer function and φ is the phase. Eq. (53) states that the modulus squared transfer function has an exponential distribution, from which it follows that the relative variance is unity. The validity of the Gaussian assumption regarding H_R and H_I can in principle be explored by using point process theory to evaluate the higher order cumulants of these quantities. The fact that $E[c_n] = 0$ implies that the fourth order cumulants can be expressed in terms of only the first and second order cumulants of the point process, g_1 and g_2. However, the analysis becomes very involved for all but the case of Poisson natural frequency spacings, in which case Lyon [3] has shown that rather than being unity, the relative variance of the modulus squared transfer function is given by

$$r_{|H|^2}^2 = 1 + \frac{K^2}{\pi m}, \tag{56}$$

so that unity is obtained at high values of m. In comparison, the Weaver result [9], Eq. (18), yields the following for the case $L = N = 1$.

$$r_{|H|^2}^2 = 1 + \frac{(K^2 - 3)}{\pi m}. \tag{57}$$

For a two-dimensional system such as a plate, the value $K = 2.25$ should be used in Eq. (56), and $K = 3$ should be used in Eq. (57)—the coefficients of the $(1/\pi m)$ term then differ by around 20%, so that the two estimates of the relative variance are fairly similar; the coefficients differ by a greater amount, 89%, for a three-dimensional system. No further analysis of the point-to-point transfer function is considered here but a detailed study has been provided by Lobkis et al. [10], in which it is shown that Eqs. (56) and (57) tend to envelope the true result for a three-dimensional system.

4. Numerical simulations

4.1. The system considered

In order to assess the validity of the foregoing analytical results, numerical simulations of a mass-loaded simply supported rectangular steel plate have been performed. The plate is taken to have plan dimensions 1.35 m × 1.2 m and thickness 5 mm, and ten point masses are attached to the surface of the plate, each having 1.5% of the total mass of the bare plate. The plate is modelled by

using the Lagrange–Rayleigh–Ritz technique, with the modes of the bare simply supported plate employed as basis functions. Typically, a sufficient number of basis functions are included to allow accurate modelling of at least the first 400 modes of the plate. A constant loss factor η is employed, so that the modal overlap factor $m = \omega\eta n$ increases linearly with frequency (the modal density n being independent of frequency for a plate). The frequency dependent results that follow are plotted as a function of m rather than as a function of ω, since the foregoing analysis identifies m as the key parameter affecting the response statistics. By selecting the location of the masses at random from a uniform distribution, it is possible to build up an ensemble of random plates so that the response statistics can be computed; typically an ensemble size of 5000 has been employed in what follows.

4.2. Natural frequencies and mode shapes

The probability density function (PDF) of the spacings between the natural frequencies is shown in Fig. 1 for a bare plate, and in Fig. 2 for a mass-loaded plate. An ensemble of one is involved in each case, since the results have been found by simply computing the first 993 modes of a single plate. Clearly, the spacings for the bare plate have an exponential distribution, which is consistent with a Poisson model of the natural frequencies, whereas those of the mass loaded plate are well approximated by a Rayleigh distribution. These results are consistent with the findings of random matrix theory [5]. The bare plate is in many ways a special case—it can be thought of as a series of uncoupled waveguides, with nothing to prevent the natural frequencies of two waveguides becoming arbitrarily close. The added masses have the effect of coupling the waveguides, and the veering phenomenon then acts to prevent the occurrence of very closely spaced natural frequencies; very little coupling is actually required to effect the transition from exponential to Rayleigh spacings. The bare plate is not considered further in the present work since Lyon's theory [3] can be considered to be highly accurate for this case; most real systems will tend to have Rayleigh natural frequency spacings.

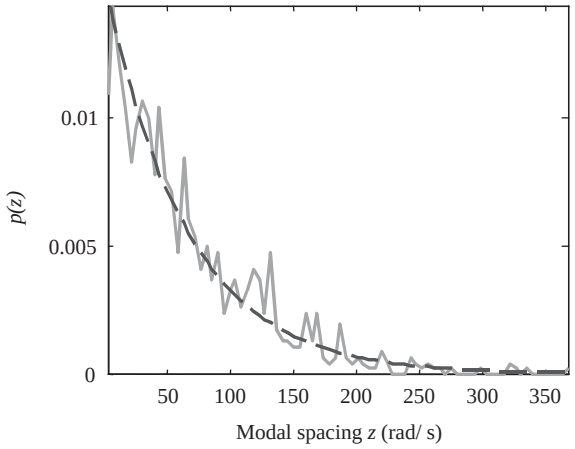

Fig. 1. PDF of natural frequency spacings, $p(z)$, for a bare rectangular plate with 993 modes considered: ——, simulation; – –, exponential PDF.

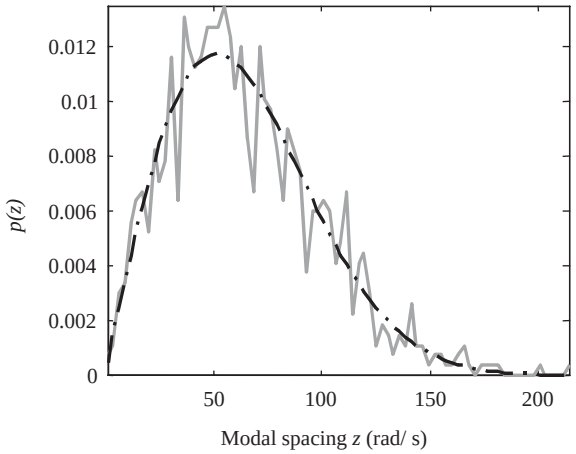

Fig. 2. PDF of natural frequency spacings, $p(z)$, for a mass loaded plate with 993 modes considered: ——, simulation; – · –, Rayleigh PDF.

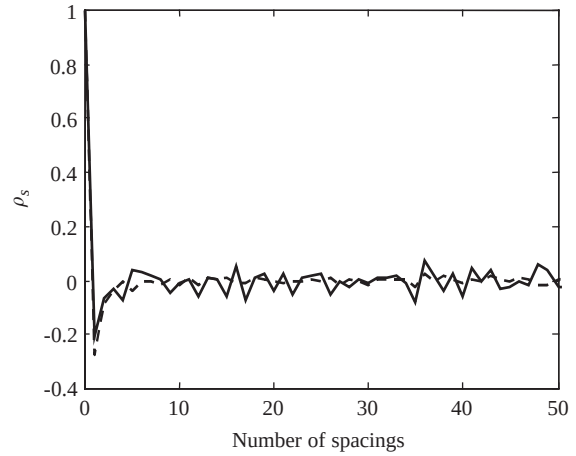

Fig. 3. Correlation function of the natural frequency spacings for a mass loaded plate with 2014 modes considered, compared to the correlation function associated with a 100∗100 member GOE: ——, Plate correlations; – –, GOE correlations.

The correlation function of the natural frequency spacings can be defined as

$$\rho_s = \frac{E[(z_j - \bar{z})(z_{j+s} - \bar{z})]}{E[(z_j - \bar{z})^2]}, \tag{58}$$

where z_j is the jth spacing and $\bar{z}$ is the mean value. This is shown in Fig. 3 for the mass loaded plate, where in this case 2014 modes have been considered in the calculation and the averages have been taken over j rather than across an ensemble. Also shown in the figure is the correlation function computed for the eigenvalues of a random matrix with GOE [5] statistics. In some ways it is surprising that the two results agree so closely, since the matrices governing the plate dynamics

have a very different form to the GOE. However, this type of agreement is much observed in practice, although it remains something of a mystery why the GOE results should be so universally valid [5].

The 55th mode shape of the mass loaded plate (with one particular configuration of the masses) is shown in Fig. 4. It can be seen that the mode shape has a highly complex spatial pattern, and the probability density function (taking a fine grid of sample points over the surface of the plate) appears to be near-Gaussian, as shown in Fig. 5. However, the quantity $\langle \phi_j^4 \rangle / \langle \phi_j^2 \rangle^2$ is shown in

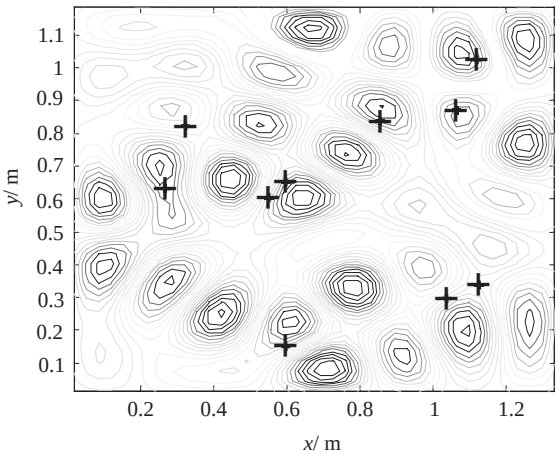

Fig. 4. 55th mode shape of a rectangular plate with 10 randomly placed masses, each having 1.5% of the plate mass. Mass positions are marked "+".

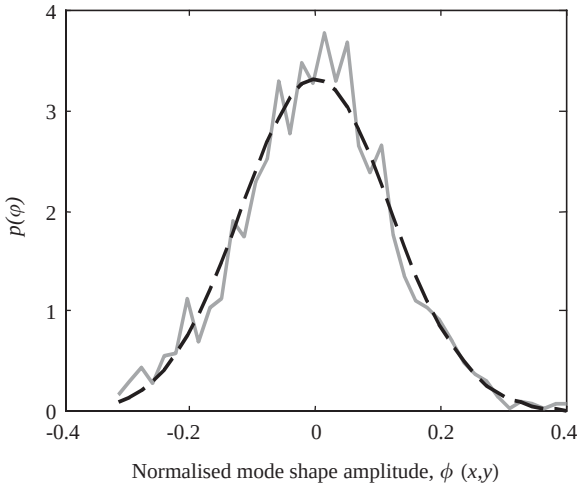

Fig. 5. Spatial PDF of the 55th mode shape of a mass loaded rectangular plate, compared with a Gaussian PDF. Spatial factor $K = 3.01$. ——, plate PDF; – –, Gaussian PDF.

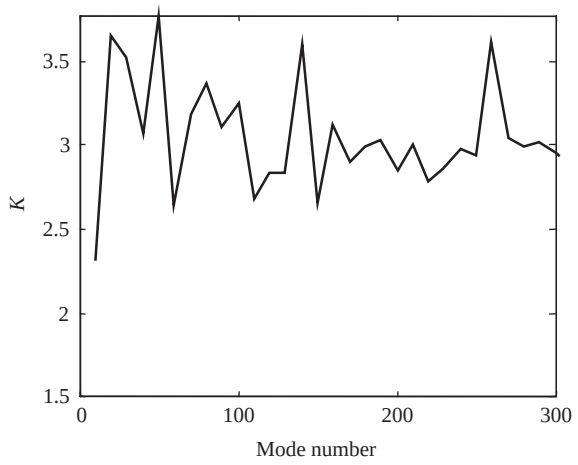

Fig. 6. Single sample result for the spatial factor K as a function of frequency ordered mode number, calculated over a grid of 10,000 points on a mass loaded plate.

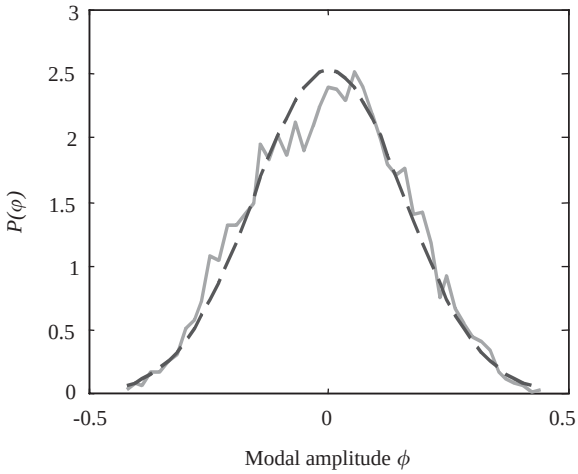

Fig. 7. Ensemble PDF at a fixed point across a 5000 member ensemble of 220th mode shape of a mass loaded plate compared with a Gaussian PDF. Spatial factor $K = 2.5$. ——, plate PDF; – –, Gaussian PDF.

Fig. 6 for a number of the modes below $j = 300$, and it can be seen that the results often fall below the Gaussian value of 3 (the mean value for modes 50–300 is 2.86). It should be noted that Figs. 5 and 6 relate to the *spatial* variation of a mode shape on one particular realization of the random structure, and not the *ensemble* variation of the mode shape at a fixed point, which is strictly required in Eq. (19). To investigate whether the mode shape statistics are ergodic, the probability density function of mode 220 at a fixed point, across an ensemble of plates, is shown in Fig. 7. Although the result appears to be near-Gaussian, the value of K is actually found to be 2.52, and repeating this exercise for a selection of modes leads to the results shown in Fig. 8. There is a clear

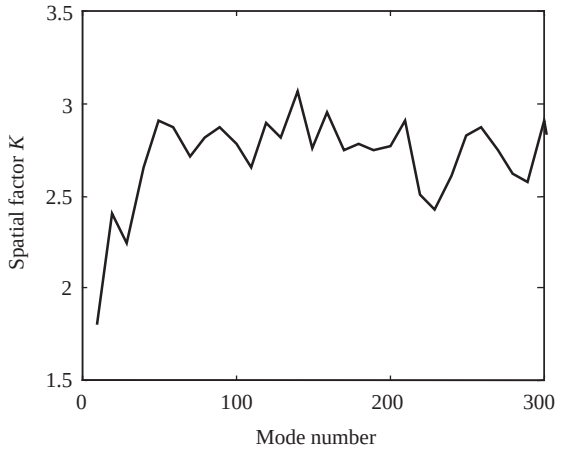

Fig. 8. Ensemble result for the spatial factor K as a function of frequency ordered mode number for a mass loaded plate. The mode shape at a fixed point across a 5000 member ensemble is considered.

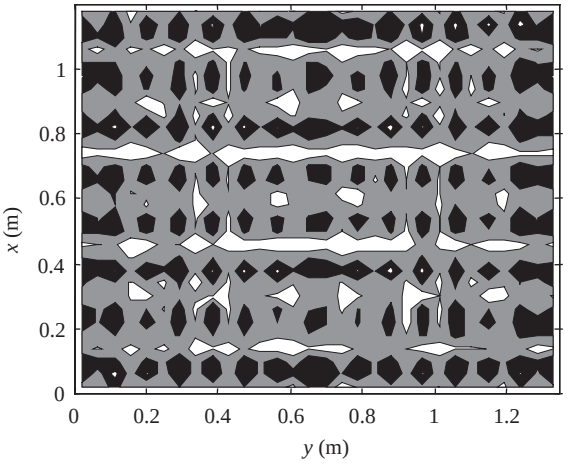

Fig. 9. Filled contour plot showing the ensemble value of the spatial factor K for mode 255 over a 5000 member ensemble of a mass loaded plate. The masses are placed randomly over the whole plate. □, $K > 2.8$; ■, $2.6 < K < 2.8$; ■, $K < 2.6$.

tendency for K to be less than 3 (in this case the mean value for modes 50–300 is 2.74), and this agrees with the findings of Lobkis et al. [10]. Another way to examine this issue is to consider the way in which K varies with the observation point, for a given mode. A contour plot of K is shown in Fig. 9 for mode 255, and for comparison, corresponding results are shown in Fig. 10 for the case in which the point masses are restricted to the left half of the plate. Little can be deduced from these figures other than the fact that K is a complex function of the spatial position, and there is a strong tendency for K to be less than 3; in fact the average value of K is around 2.67 for Fig. 9. The contours of K tend to be aligned to the plate boundaries, which suggests there may be something special about the fact that the plate is rectangular—it would be interesting for a future study to consider a less regular shape.

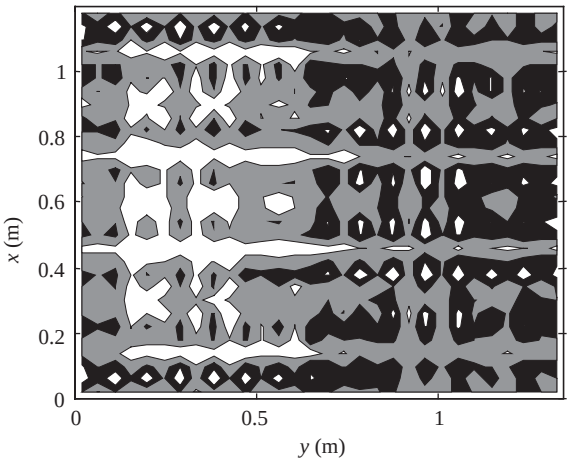

Fig. 10. Filled contour plot showing the ensemble value of the spatial factor K for mode 255 over a 5000 member ensemble of a mass-loaded plate. The masses are placed randomly over the left half of the plate only. □, $K > 2.8$; ■, $2.6 < K < 2.8$; ■, $K < 2.6$.

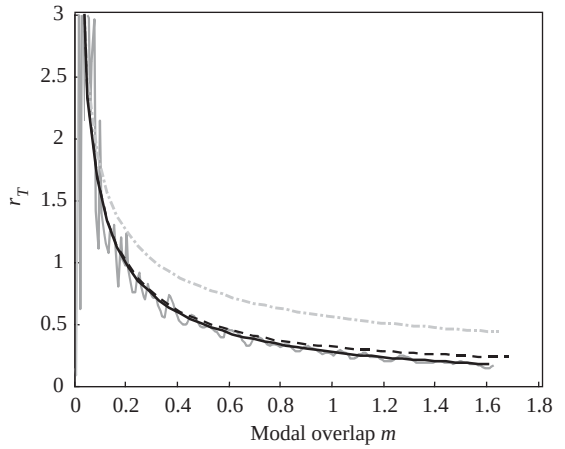

Fig. 11. The relative standard deviation of the energy density r_T for $\eta = 0.008$, 5000 member ensemble, rain-on-the-roof excitation: ——, mass loaded plate simulation; – – –, Rayleigh spacing prediction; –·–·–, Poisson prediction; ——, GOE prediction.

4.3. Energy variance: rain-on-the-roof forcing

Results for the relative standard deviation r_T of the plate kinetic energy are shown in Figs. 11 and 12 for the case of rain-on-the-roof forcing. The energy is a function of frequency, but it is plotted here as a function of modal overlap: in Fig. 11 the loss factor has been selected to give a maximum modal overlap factor of 1.6, while a higher loss factor leading to a maximum modal overlap factor of 6 has been employed in Fig. 12. In each case the frequency range covers the first 416 modes of the plate. In addition to the simulation results the figures show the Poisson prediction, Eq. (12), the Rayleigh prediction, Eq. (29), and the present GOE prediction, Eq. (40),

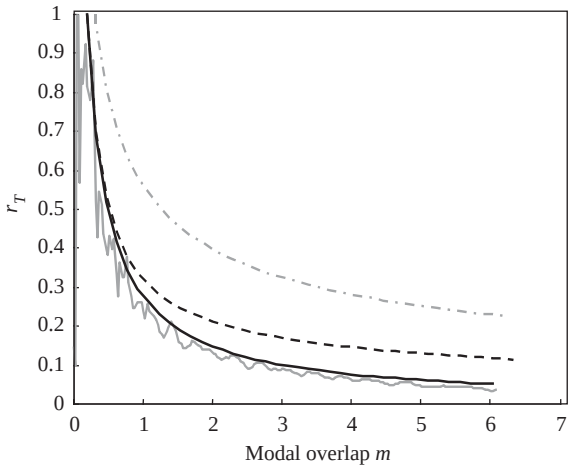

Fig. 12. The relative standard deviation of the energy density r_T for $\eta = 0.03$, 5000 member ensemble, rain-on-the-roof excitation: ——, mass loaded plate simulation; – – –, Rayleigh spacing prediction; –·–·–, Poisson prediction; ——, GOE prediction.

with $\alpha = 1$ in each case. The Poisson prediction is poor, as would be expected given the fact that the natural frequency spacings are not Poisson (see Fig. 2). In contrast the GOE prediction is in very good agreement with the simulations. The difference between the Rayleigh and GOE results is a measure of the importance of the correlation between the natural frequency spacings—this is assumed to be zero in the Rayleigh model but, as shown in Fig. 3, ρ_1 has a significant negative value. The results shown in Figs. 11 and 12 demonstrate that the correlation reduces the variance, and that this effect becomes more significant with increasing modal overlap. It is logical that the inclusion of correlations will reduce the variance, since ρ_1 will reduce the likelihood that two neighbouring spacings will be small, thus reducing the tendency for the modes to bunch and produce unusually high response levels. It is also logical that the effect will become more important at higher values of modal overlap, since the average number of modes contributing to the response at a given frequency is m—the greater the number of contributing modes, the more significant will be the effect of correlation between their modal frequencies.

4.4. Energy variance: point forcing

Figs. 13 and 14 are similar to Figs. 11 and 12, but in this case the response to point forcing is shown. The theoretical predictions now have $\alpha = K$, where K is taken to be 2.25 for the Poisson model and 3 for the Rayleigh and GOE models. In this case the three theoretical predictions are all fairly close, and all tend to overestimate the simulation results. It is interesting to note that correlation effects are less in evidence than for rain-on-the-roof excitation, since the Rayleigh and GOE predictions are in close agreement. This can be related to Eq. (29), where the second term in the integral gives the "non-Poisson" element of the Rayleigh prediction: for $\alpha = 3$ this has a less significant contribution than for $\alpha = 1$, and hence more subtle effects such as correlations can also be expected to reduce. Physically, the modal contributions to the response in Eq. (3) have random

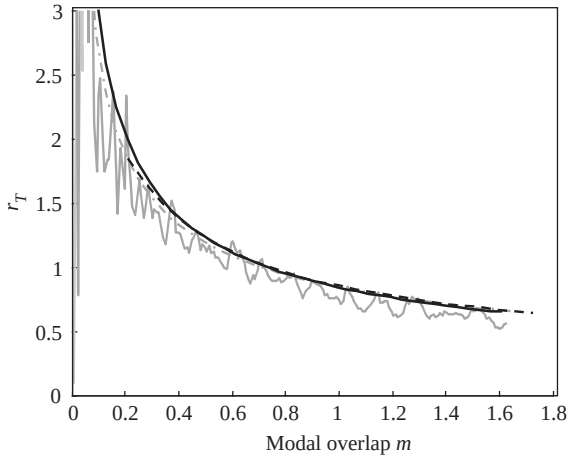

Fig. 13. The relative standard deviation of energy density r_T for $\eta = 0.008$, 5000 member ensemble, excitation at a single fixed point. ——, mass loaded plate simulation; – ·, Rayleigh spacing prediction; -·-·-, Poisson prediction; ——, GOE prediction.

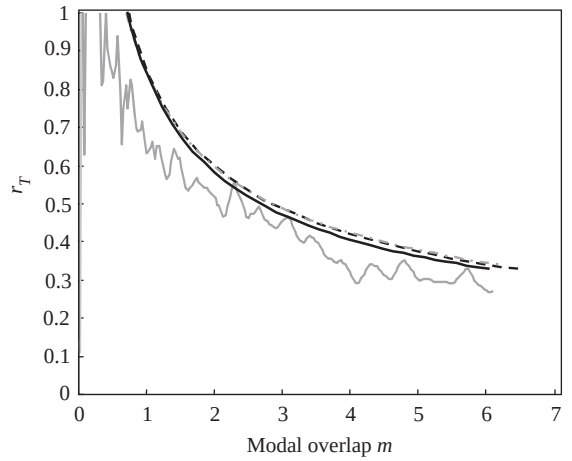

Fig. 14. The relative standard deviation of energy density r_T for $\eta = 0.03$, 5000 member ensemble, excitation at a single fixed point. ——, mass loaded plate simulation; – –, Rayleigh spacing prediction; -·-·-, Poisson prediction; ——, GOE prediction.

amplitudes, and this effect tends to reduce the significance of the detailed spacing statistics of the modes.

As discussed in Section 4.2, $K = 3$ is likely to be an overestimate of the spatial factor, and this is confirmed by the over prediction of the variance shown in Figs. 13 and 14. A revised GOE prediction is shown in Fig. 15 using the value $K = 2.74$ based on Fig. 8, leading to closer agreement with the simulations.

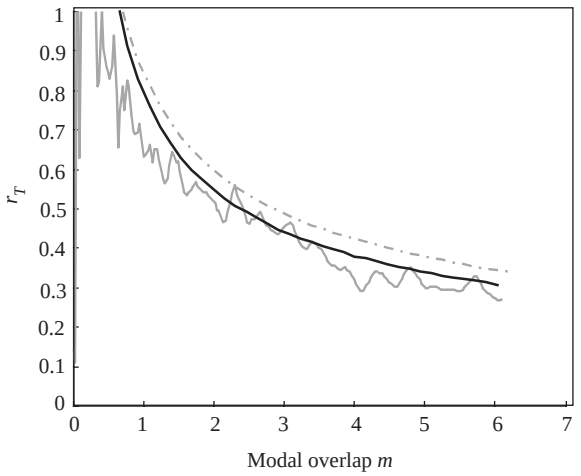

Fig. 15. The relative standard deviation of energy density r_T for $\eta = 0.03$, 5000 member ensemble, excitation at a single fixed point, compared to modified prediction: ——, mass loaded plate simulation; -·-·-, single point Lyon prediction; ——, single point GOE prediction, $K = 2.74$.

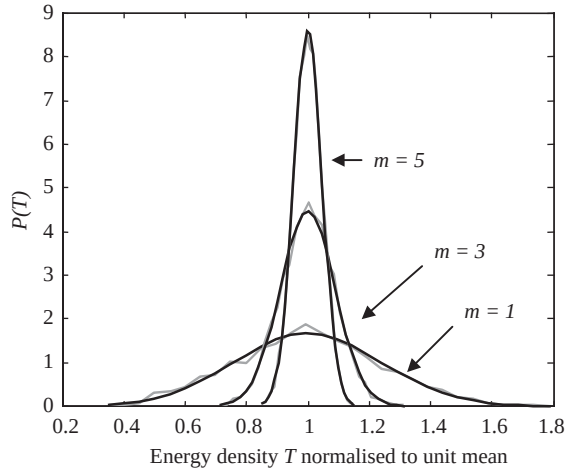

Fig. 16. Energy density PDF, $p(T)$, for a mass loaded plate excited by rain-on-the-roof forces, $\eta = 0.03$, 5000 member ensemble, at various values of the modal overlap m. ——; simulation result, ——, Gaussian PDF.

4.5. Energy statistics

Although only the mean and the variance of the energy were considered analytically in Sections 2.3 and 2.4, the simulations can be used to investigate the energy probability density function. Results are shown for rain-on-the-roof forcing in Fig. 16 and for point forcing in Fig. 17. In each case the probability density function is plotted for three values of the modal overlap factor, corresponding to three different excitation frequencies. It can be seen that the rain-on-the-roof case is well approximated by a Gaussian distribution, while the point forcing case has more the form of a Lognormal distribution. It is not possible to give a detailed analysis of these results, but

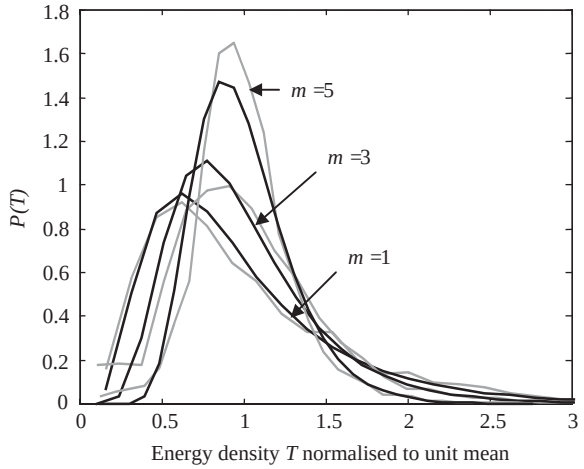

Fig. 17. Energy density PDF, $p(T)$, for a mass loaded plate excited by single fixed point force, $\eta = 0.03$, 5000 member ensemble, at various values of the modal overlap m. ——; simulation result, ——, Lognormal PDF.

some insight can be obtained by considering Eq. (17), which gives the jth cumulant of the response under the Poisson assumption. For rain-on-the-roof forcing ($a_n = 1$) the jth cumulant reduces relative to the standard deviation in accordance with $(\pi m)^{-j/2+1}$, and thus the response might be expected to become Gaussian with increasing m. This argument might also be expected to apply to the point forcing case, but perhaps the behaviour of $E[a_n^j]$ with increasing j affects the limiting process for moderate m. However, Eq. (17) is for Poisson and not GOE statistics, and a detailed explanation of Figs. 16 and 17 is not available at the present time.

5. Experimental investigation

Experiments have been performed on an aluminium plate of surface area 0.578 m^2 and thickness 1.5 mm. The plate has an irregular quadrilateral shape, so that no two edges are exactly parallel, with an approximate aspect ratio of 3:2. The general experimental arrangement is shown in Fig. 18, where it can be seen that triangular patches of damping material have been added to the plate: 3 M damping foil 2552 was employed, with an approximate area coverage of 35%. Twelve point masses, each of mass 26.2 g (approximately 1% of the plate mass), were super-glued to the reverse side of the plate in random positions. These masses could be broken off and reattached in different positions to form an ensemble of structures—in total 32 different sets of mass locations were considered. The plate was suspended on soft elastic chords, and the excitation was applied via an instrumented impact hammer. The response was measured at 22 randomly located points by using a Polytec OFV 56 scanning laser vibrometer head and an OFV 3001S vibrometer controller, the output of which was connected to a logging PC. The impact hammer was triggered automatically by using a solenoid and a pulse generator, so that five impacts (all at the same position on the plate) could be employed for each of the 22 response measurements without manual intervention—the five measurements were averaged in the frequency domain to reduce noise. The kinetic energy of the plate was then deduced by averaging the velocity squared

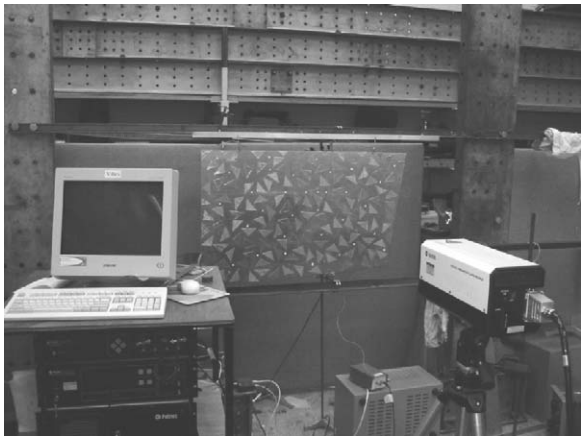

Fig. 18. Experimental set-up, showing logging PC, plate with attached damping and scanning laser vibrometer.

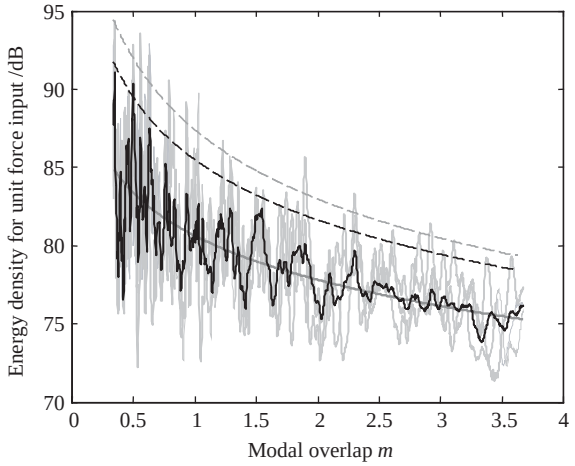

Fig. 19. Measured energy density as a function of modal overlap: ——, for typical ensemble members; ——, 32 member ensemble mean; ——, infinite system result; – – –, theoretical Gaussian 99.5% confidence interval; – – – Lognormal 99.5% confidence interval.

response over the 22 measurement points. Repeating this exercise for the 32 different mass configurations then produced an ensemble of results for the energy of the plate under single point excitation. The results were processed over the frequency range 250 Hz–2kHz, which covers around 190 modes of the plate.

In addition to the energy response measurements, the power input to the plate was measured. A power balance then enabled the loss factor η to be estimated via the formula $P = 2\omega\eta T$. It was estimated that $\eta = 0.015$, and this result was found to agree with circle-fit damping measurements on individual modes to around ± 0.005. This loss factor produces a modal overlap factor of around 3.6 at the highest frequency considered.

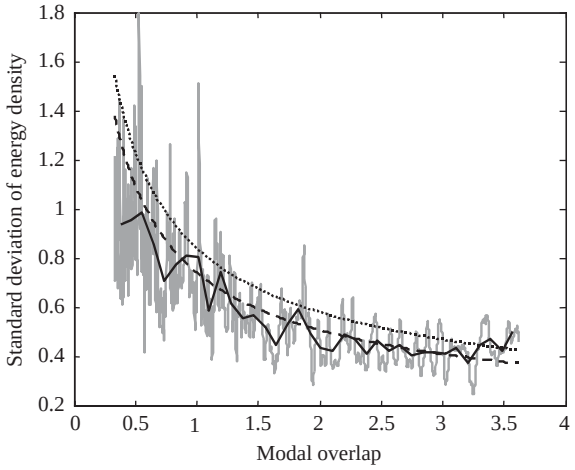

Fig. 20. Relative standard deviation of energy density for 32 member ensemble: ——, experimental result; ——, band average of experimental result; ⋯⋯, theoretical result ($K = 3$); – – –, theoretical result ($K = 2.5$).

The energy response of the plate for three of the mass configurations is shown in Fig. 19, together with measured ensemble average for all 32 configurations. Superimposed on the curves is the analytical result for the mean (effectively the standard SEA result), which is in good agreement with the measurements. Note that the limited size of the ensemble produces an oscillatory mean value rather than a smooth curve. Also shown in Fig. 19 are 99.5% confidence upper bounds based on Gaussian and Lognormal statistics—clearly the Lognormal result looks more convincing, in agreement with the results reported in Section 4.5. The measured relative standard deviation is shown in Fig. 20, both as a raw result and in band averaged form. Two theoretical predictions are shown, corresponding to Eq. (40) with $\alpha = K$ and $K = 2.5$ and 3. Clearly, the result for $K = 2.5$ is in very good agreement with the experiments, confirming the finding from the numerical simulations that the value of K is less than the theoretical Gaussian value of 3.

6. Conclusions

Three expressions have been derived for the relative variance of the energy of a system subjected to harmonic excitation. These expressions are associated with three different models of the statistics of the system natural frequencies, and are: (i) Eq. (12) for Poisson natural frequency spacings, (ii) Eq. (29) for statistically independent Rayleigh natural frequency spacings, and (iii) Eq. (40) for GOE natural frequency statistics. In each equation $\alpha = 1$ for rain-on-the-roof excitation, and $\alpha = K$ (where K depends upon the mode shape statistics) for single point excitation. Eq. (40) provides the first non-zero estimate of the variance for the case of GOE statistics with rain-on-the-roof excitation, as defined in Section 2.5.

It has been found from simulations that the natural frequencies of a mass loaded plate follow closely the GOE statistical model, and hence the GOE based variance prediction provides the closest agreement with simulation results. The assumption of statistically independent Rayleigh

natural frequency spacings neglects the spacing correlations that occur in the GOE, and this degrades the accuracy of the variance prediction at high modal overlap.

In line with previous studies it has been found that the value of the spatial parameter K is less than the theoretical Gaussian value of 3. Lobkis et al. [10] have speculated that this might be due to the occurrence of complex modes; however the present numerical simulations employed proportional damping, for which the mode shapes are real, and yet K was still found to be less than 3. The experimental value was found to be around $K = 2.5$. Clearly the precise value of K to be employed in a particular situation remains an open question.

Acknowledgements

AWMB would like to thank the Engineering and Physical Sciences Research Council for financial support under a Doctoral Studentship.

References

[1] R.H. Lyon, R.G. Dejong, *Theory and Application of Statistical Energy Analysis*, 2nd Edition, Butterworth-Heinemann, London, 1995.
[2] M.R. Schroeder, Frequency-correlation functions of frequency responses in rooms, *Journal of the Acoustical Society of America* 34 (1962) 1819–1823.
[3] R.H. Lyon, Statistical analysis of power injection and response in structures and rooms, *Journal of the Acoustical Society of America* 45 (1969) 545–565.
[4] J.L. Davy, The ensemble variance of random noise in a reverberation room, *Journal of Sound and Vibration* 107 (1986) 361–373.
[5] M.L. Mehta, *Random Matrices*, Academic Press, New York, 1991.
[6] R.L. Weaver, Spectral statistics in elastodynamics, *Journal of the Acoustical Society of America* 85 (1989) 1005–1013.
[7] C. Ellegaard, K. Schaat, P. Bertelsen, Acoustic chaos, *Physica Scripta* 90 (2001) 223–230.
[8] P. Bertelsen, C. Ellegaard, E. Hugues, Distribution of eigenfrequencies for vibrating plates, *European Physical Journal B* 15 (2000) 87–96.
[9] R.L. Weaver, On the ensemble variance of reverberation room transmission functions, the effect of spectral rigidity, *Journal of Sound and Vibration* 130 (1989) 487–491.
[10] O.I. Lobkis, R.L. Weaver, I. Rozhkov, Power variances and decay curvature in a reverberant system, *Journal of Sound and Vibration* 237 (2000) 281–302.
[11] R.L. Stratonovich, *Topics in the Theory of Random Noise*, Gordon and Breach, New York, 1963.
[12] Y.K. Lin, *Probabilistic Theory of Structural Dynamics*, McGraw-Hill, New York, 1967.
[13] S.O. Rice, in: N. Wax (Ed.), *Noise and Stochastic Processes*, Dover Publications, New York, 1951.
[14] M. Abromowitz, I.A. Stegun, *Handbook of Mathematical Functions*, Dover Publications Inc, New York, 1964.
[15] T. Shigehara, Conditions for the appearance of wave chaos in quantum singular systems with a point-like scatterer, *Physical Review E* 50 (1994) 4357–4372.
[16] S.W. McDonald, A.N. Kaufman, Wave chaos in the stadium: statistical properties of short-wave solutions to the Helmholtz equation, *Physical Review A* 37 (1988) 3067–3086.